Characteristics of a New Creep Regime in Polycrystalline NiAl

S.V. RAJ and S.C. FARMER

Constant-load creep tests were conducted on fine-grained (~23 μm) Ni-50.6 (at. pct) Al in the temperature range of 1000 to 1400 K. Power-law creep with a stress exponent, $n \approx 6.5$, and an activation energy, $Q_c \approx 290$ kJ mol^{-1}, was observed above 25 MPa, while a new mechanism with $n \approx 2$ and $Q_c \approx 100$ kJ mol^{-1} dominates when $\sigma < 25$ MPa, where σ is the applied stress. A comparison of the creep behavior of fine- and coarse-grained NiAl established that the mechanism in the $n \approx 2$ region was dependent on grain size, and the magnitude of the grain-size exponent was estimated to be about 2. Transmission electron microscopy (TEM) observations of the deformed specimens revealed a mixture of dislocation tangles, dipoles, loops, and subboundary networks in the power-law creep regime. The deformation microstructures were inhomogeneous in the $n \approx 2$ creep regime, and many grains did not reveal any dislocation activity. However, bands of dislocation loops were observed in a few grains, where these loops appeared to have been emitted from the grain boundaries. The observed creep characteristics of the low-stress region suggest the dominance of an accommodated grain-boundary sliding (GBS) mechanism, although the experimental creep rates were lower than those predicted by theoretical models by over seven orders of magnitude. The low value of Q_c in this region, which is approximately one-third that for lattice self-diffusion, is attributed to the possible existence of interconnected vacancy flow channels, or "nanotubes," at the grain boundaries.

I. INTRODUCTION

ALTHOUGH unalloyed NiAl possesses an attractive combination of oxidation, physical, and thermal properties for use in gas-turbine aircraft engines, it has poor high-temperature creep strength and low ductility at room temperatures. In addition to its potential technological importance as the base material for alloy development, binary NiAl is a model-system for studying creep mechanisms in B2 intermetallic compounds, in part due to the presence of a large solid solubility field in the Al-Ni phase diagram and in part due to it being ordered up to its melting point. The creep properties of NiAl have been studied extensively by a number of investigators for nearly three decades[1–19] and reviewed recently by several authors.[20,21,22]

The first detailed investigation of the elevated-temperature deformation mechanisms in near-stoichiometric NiAl was conducted by Vandervoort *et al.*,[11] who reported the dominance of a viscous creep mechanism with a creep stress exponent, n, of about 3.5 and a creep activation energy, Q_c, of about 290 kJ mol^{-1} above 1525 K and the occurrence of an unknown mechanism exhibiting a stress-dependent activation energy with $n > 3.5$ below this temperature. Values of $n > 3.5$ have been reported in other investigations, and a close examination of the data reveals that they fall into two broad categories: (a) $n \approx$ to 4 to 7,[6,7,9,11,13,15,16] and (b) $n \gg 7$,[4,6] depending on stress, temperature, and processing history. The reported values of Q_c from most of these investigations, for which $n \approx 4$ to 7, are generally in reasonable agreement with the activation energy for lattice self-diffusion of Ni, Q_{Ni}, in NiAl, which is about 305 kJ mol^{-1} for Ni-50 (at. pct) Al,*[23] although somewhat higher values of $Q_c \approx 325$ to 365 kJ mol^{-1} have also been reported for polycrystalline XD-processed** NiAl.[15] Based on these results and observations of subgrains (*e.g.*, Reference 11), it is generally believed that dislocation climb is the dominant creep mechanism under conditions where $n \approx 4$ to 7 and $Q_c \approx Q_l \approx Q_{Ni}$, where Q_l is the activation energy for lattice diffusion.

In addition, values of Q_c have been observed to be stress, and temperature dependent for near-stoichiometric and Ni-rich alloys.[1,6] However, the observations reported in these two studies differ from each other in some aspects. For example, Vandervoort *et al.*[11] observed that Q_c was stress dependent for Ni-50.4 Al below 1450 K for applied stresses, σ, greater than 11.0 MPa, primarily corresponding to the $n \approx 4$ to 7 region; however, Q_c was constant and equal to about Q_l above 1450 K for $\sigma <$ 11.0 MPa corresponding to the $n \approx 3.5$ region. In contrast, Yang and Dodd[6] observed that Q_c is stress dependent only below 1173 K and for applied stresses above 55.2 MPa corresponding to $n > 10$ for stoichiometric NiAl, while $Q_c \approx Q_l$ above 1173 K for $\sigma < 55.2$ MPa. The reason for this inconsistency is poorly understood at present, although it should be noted that the creep rates reported by Vandervoort *et al.*[11] are over an order of magnitude higher than those reported by other investigators.[20]

A large body of detailed microstructural observations have been conducted on NiAl single crystals.[2–5,7,17,18] In comparison, only limited data exist for polycrystalline NiAl.[6,11] In general, these observations suggest that a variety of substructural features, such as dipoles, loops, tangles, subboundaries, and subgrains, can form in NiAl

*All compositions are given in atomic percent in this article.

**XD is a trademark of the Martin Marietta Corporation, Bethesda, MD.

S.V. RAJ and S.C. FARMER, Materials Research Engineers, are with the NASA Lewis Research Center, Cleveland, OH 44135.

Manuscript submitted April 11, 1994.

under creep conditions. Although some of the microstructural studies were used as supportive-evidence in favor of a dominant creep mechanism (*e.g.*, cross slip[2,3,6] and climb[11]), the available information provides little insight on how the microstructure correlates with variations in n and Q_c as the dominant creep mechanism varies with stress and temperature.

Previous studies have been largely restricted to creep regimes where $n > 3$,[1-19] and few data exist at lower stresses, where other processes, such as diffusion creep and grain-boundary sliding (GBS) controlled processes, may dominate. Recently reported data on polycrystalline Ni-50.6 Al show a distinct transition to a new creep regime at low stresses in the temperature range of 1100 to 1300 K.[24]

The objectives of the present article are twofold: first, to report the characteristics of this low-stress creep mechanism; second, to characterize the microstructures in the low-stress and power-law creep regimes in order to understand how the microstructure varies with a change in the deformation mechanism.

II. EXPERIMENTAL

Prealloyed, vacuum-atomized NiAl powder was procured from Homogeneous Metals, Inc. (Clayville, NY). The composition of the powders (the Al and Ni contents were determined by wet chemical analysis)[25] was found to contain 50.6 pct Al and 49.4 pct Ni, with 0.011 pct C and 0.017 pct O as the major interstitial elements. The powders were sealed under vacuum in mild steel cans and extruded at 1400 K using a ratio of 16:1. The average linear intercept equiaxed grain size, d, was 22.9 ± 0.7 μm at the 95 pct confidence interval. Compression specimens of nominal dimensions 6.4 mm diameter and 12.7 mm long were machined from the extruded rods with the compression axis parallel to the extrusion direction. The specimens were tested in air under constant load between 1000 and 1400 K, with the initial stresses varying between 3.0 and 52.0 MPa. Additional data were obtained from stress-increase tests. Testing was conducted by compressing the cylindrical specimen between two superalloy or silicon-nitride pads using silicon-carbide push rods. Thin platinum or tantalum foils coated with boron nitride were placed between the ends of the specimen and the pads to minimize frictional end effects. The contraction of the specimen was measured by monitoring the displacement of an alumina extensometer attached to the ends of the push rods by a super linear capacitance transducer (SLVC). The contraction and temperature of the sample were recorded by a data acquisition system. The temperature gradient across the specimen, which was measured by three thermocouples, was typically within 1 K of the desired value.

Microstructural observations were conducted on selected tested specimens using optical microscopy, scanning electron microscopy, (SEM), and transmission electron microscopy (TEM), where the latter observations were conducted on foils cut from the gage section transverse to the stress axis. The TEM foils were prepared by jet polishing 3 mm diameter thin specimens in a solution of 70 pct ethanol, 10 pct butylcellosolve, 6 pct percholoric acid, and 14 pct distilled water at 273 K by using polishing currents and voltages of 20 to 25 V and 10 to 15 mA, respectively. The TEM microstructures of the as-extruded material were described in an earlier study.[25] These observations showed that most of the grains, as well as the grain boundaries, were essentially free of dislocations.

III. RESULTS

A. *The Shape of the Creep Curves*

Two distinct creep regimes were observed at intermediate and low stresses where the transition stress, σ_t, was about 9 to 25 MPa, depending on the absolute temperature, T. Figure 1(a) shows typical creep curves of true creep strain, ε, plotted against time, t, between 1000 and 1300 K under initial stresses varying from 12.0 to 50.7 MPa, corresponding to values above the transition stress. The nature of the primary creep curve was dependent on stress and temperature in the intermediate-stress regime, where inverse and sigmoidal primary creep transients were observed at 1000 and 1100 K, respectively, while normal primary creep occurred at 1200 and 1300 K. However, the primary creep region was generally followed by a nominally secondary regime, as shown in Figure 1(b), where the true creep rate, $\dot{\varepsilon}$, is plotted against ε. A sharp decrease in the creep rate sometimes occurred prior to the occurrence of the sigmoidal and inverse creep transients (Figure 1(b)). Noting that the as-extruded material had a completely recrystallized microstructure with few observable dislocations,[25] this initial steep drop in creep rate appears to be the result of the introduction of new dislocations in the material on loading. Inverse and sigmoidal creep transients, which have also been observed in solid-solution alloys,[26] LiF, [27] and ⟨001⟩ oriented NiAl single crystals[4,17,19] and NiAl polycrystals deformed below 1173 K[6] are generally attributed either to the inhibition of dislocation nucleation or to a low glide mobility in the material. Since dislocation nucleation is an athermal process, the transition from inverse to sigmoidal to normal primary creep in traversing from 1000 to 1200 K can be attributed to a corresponding increase in dislocation glide and climb mobility with increasing temperature.

In contrast to the behavior at intermediate stresses, normal primary creep was observed between 1100 and 1400 K below the transition stresses, and the shape of the creep curves was not dependent on temperature (Figure 2(a)). Typically, primary creep lasted over 100 hours for $\varepsilon \leq 1.5$ pct (Figure 2(b)). In general, these curves exhibited serrations at all temperatures,* although it is unclear at present whether they are genuine, due to dynamic recrystallization and grain growth similar to those

*Figure 2(a) is presented as-recorded so as to provide an unbiased viewpoint to the reader, while smooth curves are shown in Figure 2(b) for better clarity. It was necessary to smoothen these curves, because it was not possible to distinguish the genuine changes in the creep rates due to the serrations from scatter. It may be noted that these serrations were not observed for comparable creep rates at intermediate stresses.

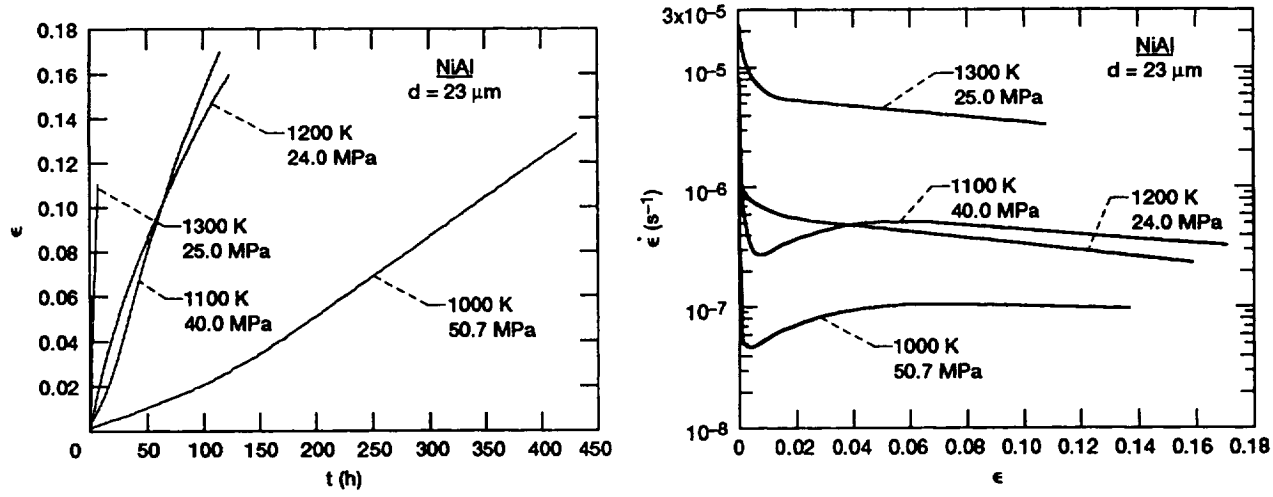

(a) (b)

Fig. 1—(*a*) True creep strain *vs* time and (*b*) true creep rate *vs* true creep strain for polycrystalline Ni-50.6 Al, tested under compressive engineering stresses and at temperatures between 24.0 and 50.7 MPa and 1000 and 1300 K, respectively.

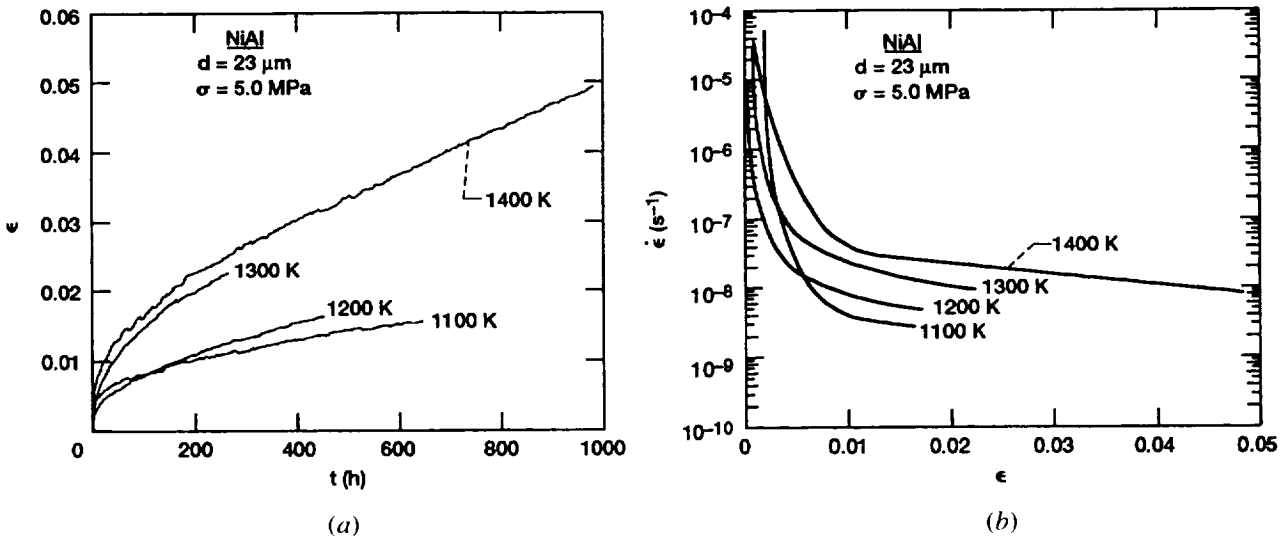

(a) (b)

Fig. 2—(*a*) True creep strain *vs* time and (*b*) true creep rate *vs* true creep strain for polycrystalline Ni-50.6 Al, tested at temperatures between 1100 and 1400 K under a compressive engineering stress of 5.0 MPa.

observed in other materials,[28] or whether they are artifacts, due to variations in room temperature during the duration of the experiment. Grain-size measurements conducted on the specimens deformed under $\sigma \approx 5.0$ MPa (Figure 2) showed that the average final grain sizes were about 35, 65, and 118 μm at 1200, 1300, and 1400 K, respectively.

B. *Stress Dependence of the Secondary Creep Rate*

Figure 3 shows the variation of the true secondary creep rate against true stress between 1000 and 1300 K. The values of creep rates in Figure 3 were obtained from the slopes of regression lines drawn through the true creep strain *vs* time data in the secondary creep region, where it was ensured that the regression data varied over small values of strain. The average true stress over this range of regressed data are reported in Figure 3. As noted previously, the creep strength of NiAl was reported to be independent of composition in the temperature range of 1200 to 1400 K.[11] These observations are also confirmed by the data shown in Figure 3, where a comparison shows excellent agreement between the present results and the compression data reported by Whittenberger for Ni-49.2 pct Al[13] and Bowman *et al.* for Ni-50.6 Al[25] for powder-extruded alloys tested under constant engineering strain rate and constant-load conditions. Using a power-law relation

$$\dot{\varepsilon} = A_1 \sigma^n \qquad [1]$$

where A_1 is a constant and n is the stress exponent; Table I gives the values of A_1, n, and the coefficient of determination, R_d^2, determined above and below the transition stress. As shown in Figure 3 and Table I, the data

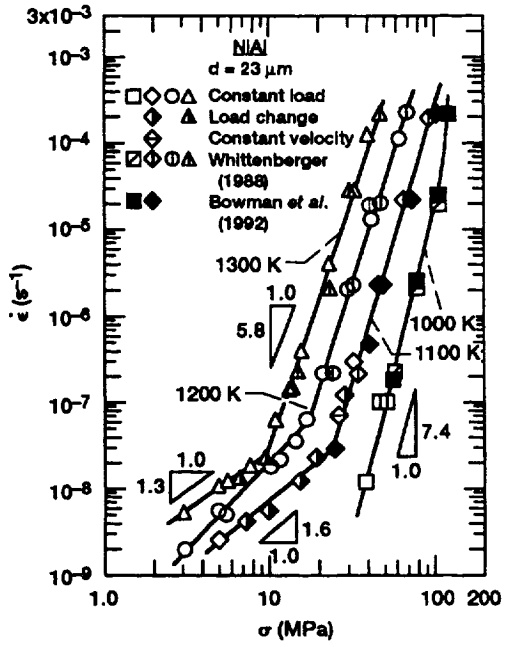

Fig. 3—Variation of the compressive true strain rate with applied true stress for Ni-50.6 Al. The data reported by Whittenberger[13] for Ni-49.2 Al and Bowman *et al.*[25] for Ni-50.6 Al are also included for comparison.

fall into two distinct creep regimes: a low-stress region with a stress exponent $n \approx 1.3$ to 2.0 and an intermediate stress region with $n \approx 5.8$ to 6.2. In addition, evidence of a third creep regime is visible in Figure 3 at high stresses above 100 MPa at 1000 K, where the data show a tendency to deviate from power-law creep behavior. There appears to be no previous report of a similarly distinct transition from power-law creep to the low-stress behavior in binary NiAl other than that observed in this study,[24] although Jung *et al.*[12] reported a change in mechanism from $n \approx 4$ to $n \approx 1$ in a coarse-grained Ni-10Fe-50Al ternary alloy below 80 MPa at 1023 K. In comparison, the transition stresses for binary NiAl, while being temperature dependent, occur below 25 MPa (Figure 3 and Table I).

C. *Temperature Dependence of the Secondary Creep Rate*

The values of n and the true activation energy for creep, Q_c, were determined both by multiple regression analysis and a graphical technique from Figure 3 using Eq. [2]:[29]

$$\dot{\varepsilon} = A_2(E/T)(\sigma/E)^n \exp(-Q_c/RT) \qquad [2a]$$

with

$$A_2 = A(D_0\mathbf{b}/\mathrm{k})(\mathbf{b}/d)^p \qquad [2b]$$

where D_0 is a frequency factor, E is the Young's modulus, $\mathbf{b}$ is the Burgers vector, k is Boltzmann's constant, R is the universal gas constant, p is the grain-size exponent, and A is a dimensionless constant. Table II gives the magnitudes of A_2, n, and Q_c determined by multiple regression analysis for the low- and intermediate-stress regimes, where Q_c has been corrected for the temperature and composition dependence of the Young's modulus, and the $1/T$ term in the pre-exponential factor in Eq. [2]. The values of Young's moduli used in this study were calculated using[30]

$$E = 259.3 - 0.072\,T + 3 \times 10^{-5}\,T^2 - 6 \times 10^{-4}\,cT \qquad [2c]$$

where c is the atomic percent of aluminum in the alloy.

It is clear from Table II that the regressed values of n are 1.7 ± 0.2 and 6.4 ± 0.4 and that those of Q_c are 98.2 ± 14.5 and 287.1 ± 25.8 kJ mol^{-1} for the low-stress and the intermediate-stress power-law creep regimes, respectively. The magnitude of Q_c, shown in Table II for the power-law creep regime, falls within the range of values between 285 and 315 kJ mol^{-1} reported in the literature for creep activation energies of binary NiAl alloys.[20,21] The reported values of Q_{Ni} determined from diffusion studies show considerable scatter for binary NiAl alloys with nominally similar composition.[21] However, a value of $Q_c \approx 290$ kJ mol^{-1} (Table II) is closer in agreement with $Q_{Ni} \approx 275$ and 305 kJ mol^{-1} observed by Hancock and McDonnell[23] for Ni-50.8 Al and Ni-50 Al, respectively. No comparable values corresponding to $Q_c \approx 100$ kJ mol^{-1} appear to have been reported in the creep and diffusion literature on NiAl. Because activation energies for creep and diffusion are similar for a large number of materials,[31] a value of 100 kJ mol^{-1} probably represents a measure of the activation energy for grain-boundary diffusion, Q_{gb}, in NiAl. If so, this value would represent the first experimental estimate of Q_{gb} in NiAl.

The true activation energy for creep was also determined from an Arrhenius semilogarithmic plot of $(\dot{\varepsilon}T/E)$ *vs* $1/T$ for different values of σ/E, where Q_c was determined from the slopes of the regression lines (Figure 4). The variation of Q_c with σ/E is plotted in Figure 5, where the error bars represent one standard deviation about Q_c. The activation energy data have been classified into three regions. Region I occurs at low stresses when $\sigma/E \leq 1.5 \times 10^{-4}$, where the average $Q_c \approx 95$ kJ mol^{-1} is in good agreement with the value of $Q_c \approx 98$ kJ mol^{-1}, determined by multiple regression analysis (Table II). Region II occurs after a transition stage when $1.5 \times 10^{-4} \leq \sigma/E < 3.0 \times 10^{-4}$, where $Q_c \approx 300$ kJ mol^{-1} is in good agreement with Q_{Ni} for Ni-50 Al[23] and the data shown in Table II and corresponds to the power-law creep regime. For $\sigma/E \geq 3.0 \times 10^{-4}$, Q_c decreases linearly with increasing σ/E in region III. A similar decrease in activation energy with increasing stress was also reported by Vandervoort *et al.*[1] and Yang and Dodd[6] for polycrystalline NiAl. Similarly, $Q_c \ll Q_l$ was observed for NiAl single crystals under constant-load tensile creep between about 750 and 1050 K, although due to limited data, the magnitudes of Q_c were not reported.[2]

The apparent activation volume for creep, V^*, can be estimated from the stress dependence of Q_c using[32,33]

$$V^* = -2(\partial Q_c/\partial\sigma)_T \qquad [3]$$

assuming $\sigma = 2\tau$, where τ is the shear stress. It should

Table I. Values of A_1 and n at Different Temperatures Determined by Regression Analysis*

T (K)	A_1 ($MPa^{-n}\ s^{-1}$)	n	R_d^2	Remarks
1000	2.7×10^{-20}	7.4 ± 0.9	0.976	For $\sigma < 125$ MPa
1100	1.9×10^{-10}	1.6 ± 0.3	0.978	$\sigma \leq 25.0$ MPa
	7.9×10^{-17}	6.2 ± 0.5	0.987	$\sigma > 25.0$ MPa
1200	1.9×10^{-10}	2.0 ± 0.4	0.984	$\sigma \leq 16.3$ MPa
	3.1×10^{-15}	5.9 ± 0.5	0.988	$\sigma \geq 16.3$ MPa
1300	1.2×10^{-9}	1.3 ± 0.4	0.956	$\sigma \leq 9.4$ MPa
	5.2×10^{-14}	5.8 ± 0.4	0.991	$\sigma > 9.4$ MPa

*The values of error represent 95 pct confidence intervals.

Table II. Magnitudes of A_2 Parameter, Stress Exponent, and the True Activation Energy for Creep at Low and Intermediate Stresses Determined by Multiple Regression Analysis of the Creep Data Using Equation [2a]*

	T (K)	A_2 ($m^2\ K\ N^{-1}\ s^{-1}$)	n	Q_c (kJ mol^{-1})	R_d^2
Intermediate stresses	1000 to 1300	8.7×10^{22}	6.4 ± 0.4	287.1 ± 25.8	0.957
Low stresses	1100 to 1300	3.5×10^{-5}	1.7 ± 0.2	98.2 ± 14.5	0.973

*The values of error represent the 95 pct confidence intervals.

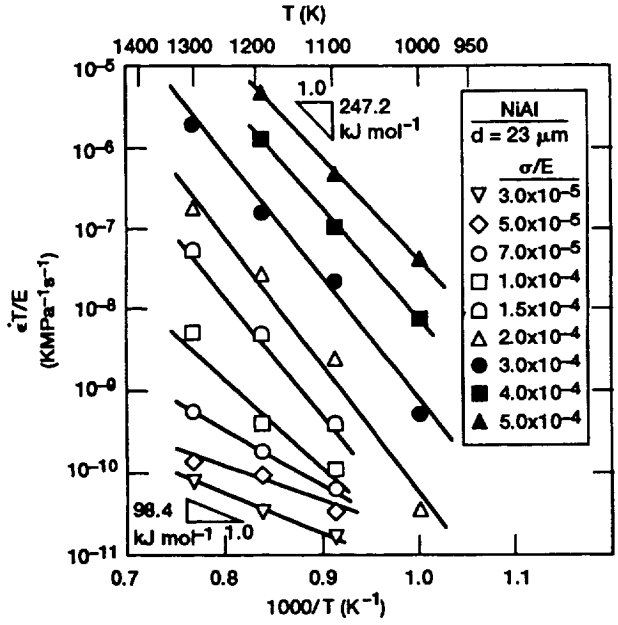

Fig. 4 — Arrhenius plot of the temperature-compensated creep rate for Ni-50.6 Al *vs* inverse of the absolute temperature for values of normalized stresses varying between 3.0×10^{-5} and 5.0×10^{-4}.

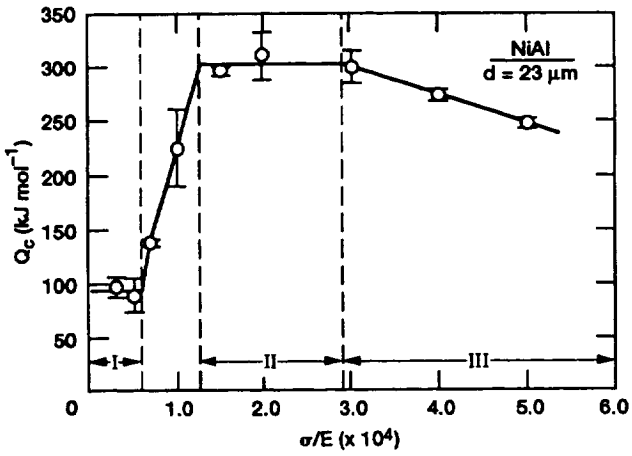

Fig. 5 — Variation of the true activation energy for creep with normalized stress showing three creep regimes in Ni-50.6 Al.

be noted that Eq. [3] is valid only when the stress dependence of the entropy term in the rate equation is negligible. Thus, from Figure 5, $V^* \approx 100\ b^3$ in region III, which compares reasonably well with the value of about 75 b^3 reported by Vandervoort *et al.*[11] at a stress of 68.9 MPa (*i.e.*, $\sigma/E \approx 4 \times 10^{-4}$).

D. *Grain-Size Dependence of the Creep Rate*

In order to verify if the mechanism in the $n \approx 2$ regime is dependent on grain size, a specimen was crept for about 1000 hours at 1400 K under an initial stress of about 5.0 MPa in order to allow the grains to grow from 23 to 117.8 ± 6.1 μm (Figure 2). The temperature was then reduced to 1200 K and the secondary creep rates were determined from stress-increase tests (Figure 6). The stress dependence of these creep rates are shown as open symbols in Figure 7, which also compares the creep behavior of the fine-grained material (solid lines from Figure 3). It is clear from Figure 7 that the creep rates for the fine- and coarse-grained specimens are in good agreement in the power-law creep regime with $n \approx 5.9$ (Table I). This observation suggests that power-law creep is independent of grain size (*i.e.*, $p \approx 0$ in Eq. 2(a)) for NiAl similar to observations reported for other materials.[26,28,29,31] However, while the fine-grained material deviates to a $n \approx 2$ type creep behavior below a stress of about 16 MPa, the coarse-grained specimen continues to exhibit a value of $n \approx 5.9$ until a stress

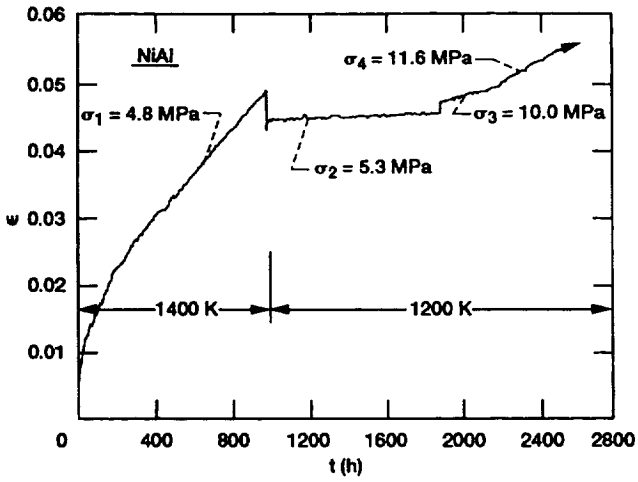

Fig. 6—Stress and temperature changes conducted on a single specimen of Ni-50.6 Al in the low-stress regime to determine the grain-size dependence of the secondary creep rate. The grain size increased from about 23 to 118 μm after the specimen was crept at 1400 K under a compressive engineering stress of 4.8 MPa. The stress changes were conducted on the coarse-grained specimen at 1200 K.

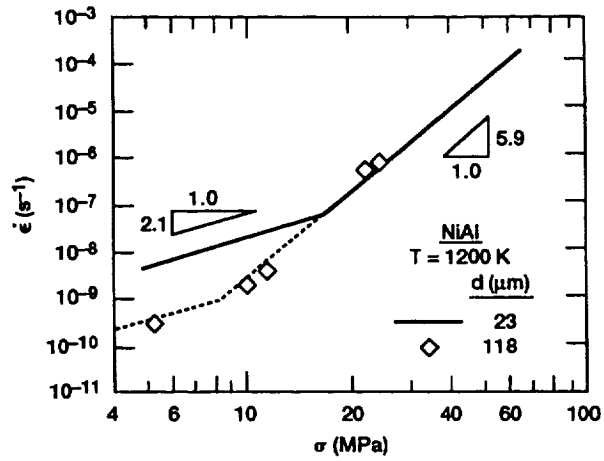

Fig. 7—Comparison of the stress dependence of the secondary creep rates at 1200 K for fine- and coarse-grained Ni-50.6 Al.

of about 9 MPa, below which a similar change in mechanism to the $n \approx 2$ regime is expected to occur. Figure 7 clearly demonstrates that the creep rate for the coarse-grained specimen in the $n \approx 2$ regime is lower than that for the fine-grained material by about a factor of 15 for $\sigma \approx 5.0$ MPa. Using the ratios of logarithmic values of the creep rates and grain sizes at 5.0 MPa, the magnitude of the grain-size exponent was estimated to be $p \approx 2$. However, this value could not be confirmed by direct measurements of secondary creep rates from tests conducted on two specimens with initial grain sizes of 10 and 23 μm deformed at 1200 K under an initial stress of 4.9 MPa due to significant grain growth in the former to about 20 μm during creep (Figures 8(a) and (b)). However, the fine-grained specimen exhibited higher creep strains at identical creep times (Figure 8(a)) and crept at much faster rates in the primary creep region (Figure 8(b)) than the coarse-grained material.

E. *Microstructural Observations*

1. *Power-law creep regime*

Transmission electron microscopy of crept specimens showed a mixture of subboundaries, cells, dislocation dipoles, loops, tangles, and random dislocations at stresses corresponding to the power-law creep region with $n \approx 6.5$ (Table II). It is interesting to note that the substructure often appeared to vary with grain size within the same TEM foil: small grains appeared to possess smaller subgrains and a higher dislocation density than larger grains. This observation suggests that the localized stresses in the smaller grains were larger than in the coarser grains. Figure 9(a) shows a distribution of subgrains in a specimen deformed to a true strain of 17.3 pct at 1200 K under a stress of 41.3 MPa. The subgrains were generally larger than the field of view even at low magnifications, and they were estimated to be about 10 μm. This value compares well with a calculated equilibrium subgrain size of $d_s \approx 11$ μm based on the subgrain size-stress relationship.[34] Individual dislocations and dislocation tangles are evident within the subgrains in Figures 9(a) through (c), where some of the isolated dislocations appear zigzag in shape (*e.g.*, at A in Figure 9(b)). Recent calculations suggest that dislocations with negative line tensions can attain these shapes in NiAl in order to minimize the forces acting on them when in equilibrium if the angle between the Burgers vector and the dislocation line vector is less than 13 deg.[35] Most of the dislocations had a ⟨100⟩ Burgers vector, with the glide planes being either {100} or {110}. Hexagonal dislocation networks consisting of three ⟨100⟩ type dislocations were sometimes observed. In many other instances, dipoles (*e.g.*, B) and loops (*e.g.*, C) were evident within the subgrains (Figure 9(d)).

2. *Low-stress creep regime*

A variety of dislocation substructures was observed in the $n \approx 2$ region, and the microstructure was very heterogeneous. Ill-formed cells, dipoles, loops, dislocation tangles, and dislocation networks formed at stresses corresponding to the upper end of the $n \approx 2$ region. For example, Figure 10(a) shows a mixture of hexagonal networks and dislocation tangles, while Figure 10(b) shows a rudimentary cellular microstructure in a specimen deformed to a true strain of 2.7 pct at 1200 K under a stress of about 9.8 MPa. Dislocation loops and tangles (Figure 11(a)) and a mixture of hexagonal networks, dipoles, and zigzagged dislocations (Figure 11(b)) are seen in another sample deformed to a true strain of 7.2 pct at 1200 K under a stress of 14.1 MPa.

In contrast, no substructure was evident in most of the grains in a specimen deformed to a true strain of 3.1 pct at 1200 K under an initial stress of 5.4 MPa, corresponding to the lower end of the $n \approx 2$ region (Figure 12(a)), although bands of dislocation loops were seen within a few grains (Figure 12(b)). Similar observations were also made at 1300 K, thereby suggesting that these results, consisting of a mixture of grains with no dislocation substructure and a few grains with bands of dislocation loops, are representative of the microstructure in the $n \approx 2$ region. As noted previously, the

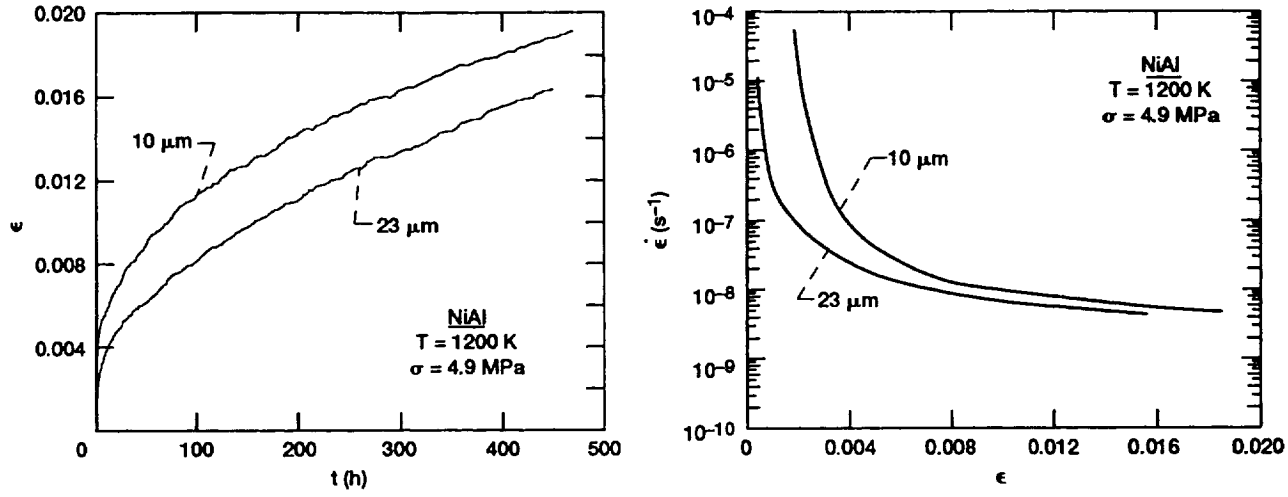

Fig. 8—(*a*) True creep strain *vs* time and (*b*) true creep rate *vs* true creep strain for polycrystalline NiAl, tested under a compressive engineering stress of 4.9 MPa at 1200 K for specimens with initial grain sizes of 10 and 23 μm.

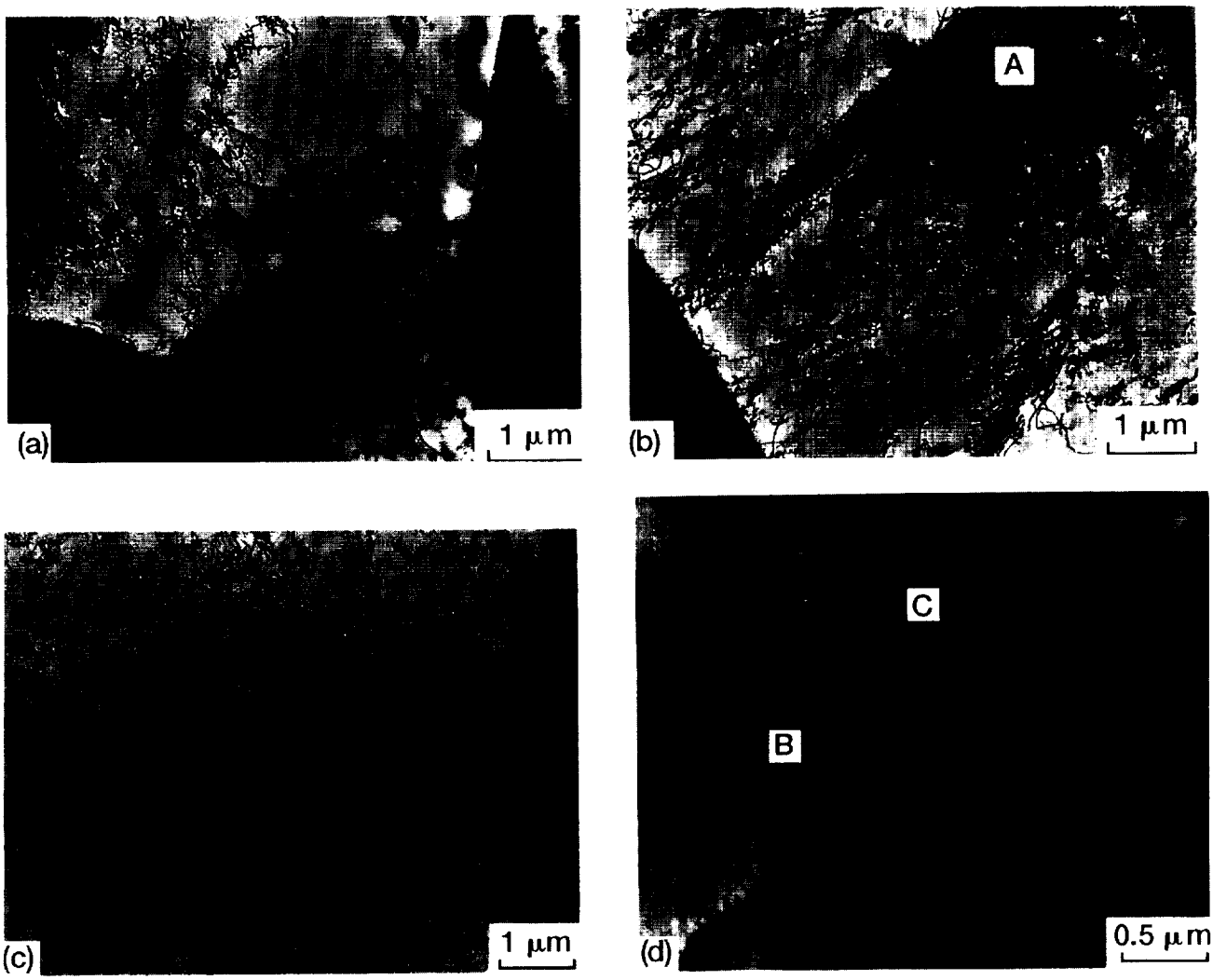

Fig. 9—TEM of crept Ni-50.6 Al showing (*a*) a distribution of subgrains containing isolated dislocations and dislocation tangles, (*b*) and (*c*) dislocation tangles and zigzagged dislocations (*e.g.*, at A in (*b*)), and (*d*) dipoles (*e.g.*, at B) and loops (*e.g.*, at C). (a), (b), and (c), T = 1200 K, σ = 41.3 MPa, and ε = 17.3 pct; and (d) T = 1200 K, σ = 29.2 MPa, and ε = 19.9 pct.

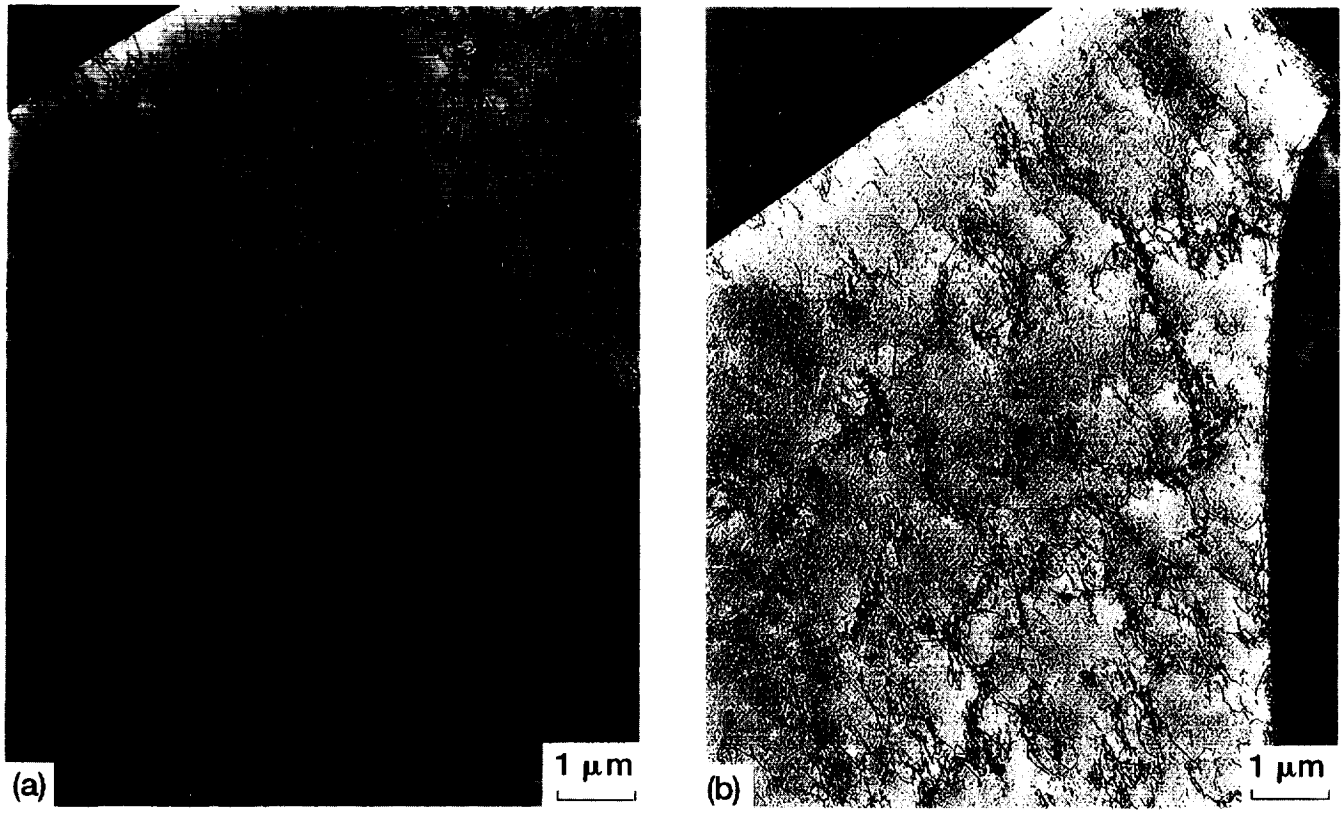

Fig. 10—TEM of a Ni-50.6 Al specimen crept to a true strain of 2.7 pct at 1200 K under a compressive engineering stress of 9.8 MPa showing (*a*) a distribution of hexagonal networks and dislocation tangles and (*b*) dislocation cells.

initial microstructure of the extruded material showed little or no evidence of dislocation activity either in the matrix or in the grain boundaries.[25] Therefore, it is suggested that these bands of loops may be dislocation debris resulting from the deformation process. A close examination of the grain-boundary regions showed considerable evidence of dislocation activity in a number of grain boundaries at both 1200 and 1300 K, where several grain boundaries also showed the presence of extrinsic grain-boundary dislocations of two different characters (Figure 12(c)). These grain-boundary dislocations were often sharply zigzagged, possibly due to the effect of anisotropy on the dislocation line tension.[35] Several dislocation loops oriented parallel to the grain boundary also can be seen in Figure 12(c), where several of these elongated loops appear to be in the process of pinching off into smaller loops.

Preliminary observations suggested that the grain boundaries were the source for these dislocation loops in the matrix presumably to accommodate GBS during creep (Figure 13). A close examination of Figure 13(a) shows the formation of dipoles at the grain boundaries; these dipoles pinch off to emit loops into the matrix (Figure 13(b)). As evident in Figures 13(a) and (b), the generation of the dipoles appeared to have resulted from a dislocation reaction in the grain boundary. It should be noted that the loops in the matrix are often elongated, and, in many cases, they seem to be in the process of pinching off into smaller loops (Figures 12(c) and 13(a) and (b)). While observations such as those shown in Figure 13 were confirmed to be genuine dislocation emissions from the grain boundaries, it should be noted that other similar observations proved to be artifacts of imaging, because careful tilt experiments performed within the TEM showed that the "emitted" loops were not always in contact with the grain boundary.

IV. DISCUSSION

The present results indicate the existence of three creep regions in NiAl (Figure 5). Region I, which occurs at low stresses, is characterized by $n \approx 2$, $Q_c \approx 100$ kJ mol^{-1}, and $p \approx 2$. Power-law creep occurs in region II at intermediate stresses with $n \approx 6.5$, $Q_c \approx 290$ kJ mol^{-1}, and $p \approx 0$, while region III occurs at high stresses where n and Q_c are stress dependent. Figure 14 shows these three creep regions in a plot of normalized creep rate, $\dot{\varepsilon} \exp(Q_c/RT)(kT/D_0E\mathbf{b})(\mathbf{b}/d)^p$, against normalized stress, σ/E, where the creep data shown in Figure 3 was normalized by using Eq. [2]. Additional data obtained below 1000 K[25] are also included in the figure in order to clearly distinguish region III. The normalization parameters used in regions II and III are $D_0 = 1 \times 10^{-4}$ m^2 s^{-1}, $Q_c = 290$ kJ mol^{-1} (Table II), and $p = 0$ and $\mathbf{b} = 0.2876$ nm. The magnitude of D_0 was chosen arbitrarily to lie between experimentally determined values for Ni-50 Al ($D_0 = 4.5 \times 10^{-4}$ m^2 s^{-1}) and Ni-50.8 Al ($D_0 = 2.3 \times 10^{-5}$ m^2 s^{-1}).[23] Other values of D_0 will shift the data parallel to the vertical axis. For

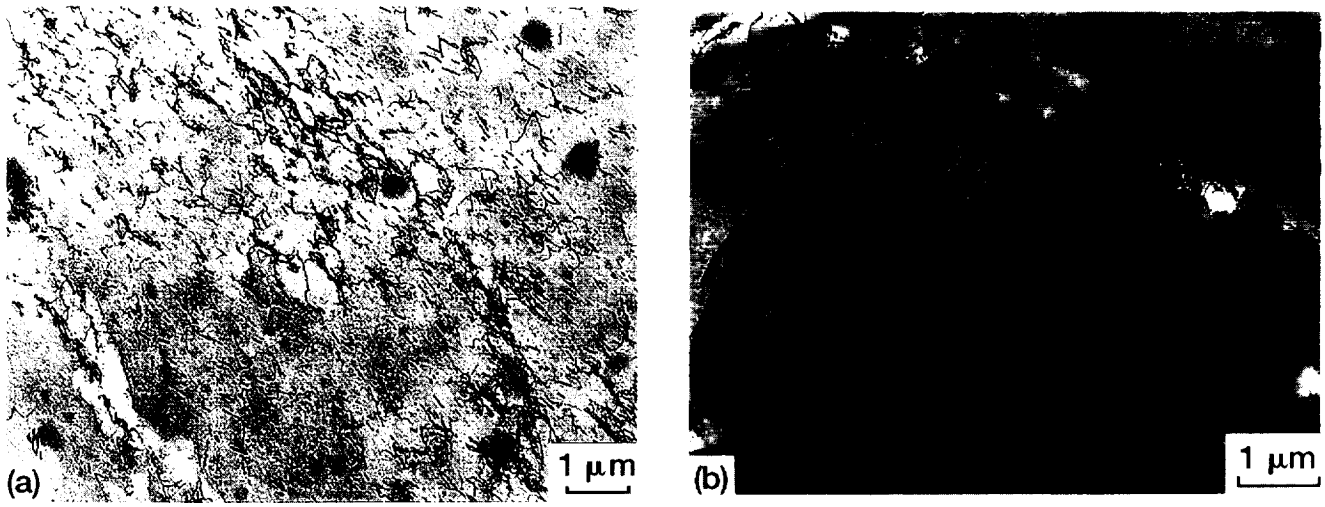

Fig. 11—TEM of a Ni-50.6 Al specimen crept to a true strain of 7.2 pct at 1200 K under a compressive engineering stress of 14.1 MPa showing (*a*) dislocation loops and tangles and (*b*) a mixture of hexagonal networks, dipoles, and zigzagged dislocations.

simplicity, the stress dependence of the activation energy observed in region III (Figure 5) is ignored in this normalization so that the data in this regime show a higher degree of scatter than in the other two regions. The creep rates in region I were normalized with $D_0 = 3.7 \times 10^{-3}$ m^2 s^{-1}, $Q_c = 100$ kJ mol^{-1}, and $p = 2$. In Figure 14, regions I, II, and III occur below $\sigma/E \approx 8 \times 10^{-5}$, between $\sigma/E \approx 8 \times 10^{-5}$ and 4×10^{-4}, and above $\sigma/E \approx 4 \times 10^{-4}$, respectively. Linear regression analysis of the normalized data corresponding to regions I and II gave $n \approx 1.7 \pm 0.2$ and 6.3 ± 0.2, respectively, which are consistent with the values shown in Table II. The values of A for regions I and II were evaluated to be 1.9×10^{-6} ($R_d^2 = 0.945$) and 1.7×10^{13} ($R_d^2 = 0.984$), respectively. The power-law relation breaks down for $\sigma/E > 4 \times 10^{-4}$ in region III (Figure 14).

The microstructural observations reported in this article are summarized schematically in Figure 15 with relation to the normalized data shown in Figure 14. The calculated values of d_s[134] shown at the top of Figure 15 suggest that subgrains are expected to be observed mainly at normalized stresses for which $d_s < d \approx 23$ μm. As shown in Figure 15, a variety of substructural features is observed over the range of stresses and temperatures studied, which correspond to regions I and II. At the upper end of region II, a mixture of sub-boundaries, random dislocations, dislocation tangles, dipoles, and cells are observed. At the other extreme, corresponding to low normalized stresses well within region I, where $n \approx 2$, most of the grains are free of any substructural features Figure 12(a), although bands of dislocation loops were observed in some grains (Figure 12(b)). Although dislocation tangles and networks are observed at the upper end of region I, it is clear from Figure 15 that these specimens were deformed under conditions close to the transition point between regions I and II, so that these substructures may not be truly representative of region I. The absence of substructure in most of the grains and the presence of bands of dislocation loops in some grains is believed to more accurately represent the microstructure in region I. Since the main scope of this study was to understand the characteristics of region I and most of the data were obtained in regions I and II, no microstructural study was conducted in region III. Thus, no specific comment can be made regarding the nature of the microstructure that forms in this region. However, elongated dislocation loops, tangles, and sub-boundaries were observed in coarse-grained polycrystalline NiAl containing 49 to 51 pct Al in an earlier study under conditions that appear to correspond to the transition regime between regions II and III.[16]

The results obtained in this study are insufficient to identify the mechanisms dominant in region III and only general comments can be made regarding them. As mentioned in Section I, although a stress-dependent activation energy was reported in two earlier studies,[1,6] the two sets of data are inconsistent. Based on Figures 3 and 5, as well as on the data shown in Figure 14 corresponding to region III,[125] the present results support the observations of Yang and Dodd,[6] who reported that Q_c varies inversely with increasing stress only below 1173 K, where $n \gg 7$. As noted in Section III–C, a value of $V^* \approx 100$ **b**^{3} was estimated from the stress dependence of Q_c in region III (Figure 5). Because $V^* \approx 1$ to 20 **b**^{3} for a Peierls–Nabarro mechanism,[33] the latter process does not appear to be important in region III under the stress and temperature conditions studied in the present investigation. Noting that $V^* \approx 10^2$ to 10^4 **b**^{3} and 10 to 10^2 **b**^{3} for obstacle-controlled glide and cross slip dominated deformation processes, respectively,[32,33] the estimated value of V^* suggests that either or both of these mechanisms may contribute significantly to the total creep rate in region III. In this regard, some of the early microstructural observations reported evidence of dislocation cross-slip in crept NiAl single and polycrystals.[2,3,6] However, systematic microstructural studies need to be conducted to characterize region III.

The values of $n \approx 4$ to 7 and $Q_c \approx Q_l$ reported in this and other investigations[6,7,9,11,13] would suggest that a dislocation climb mechanism is dominant in region II. This conclusion is consistent with observations on pure metals and solid-solution alloys exhibiting class M

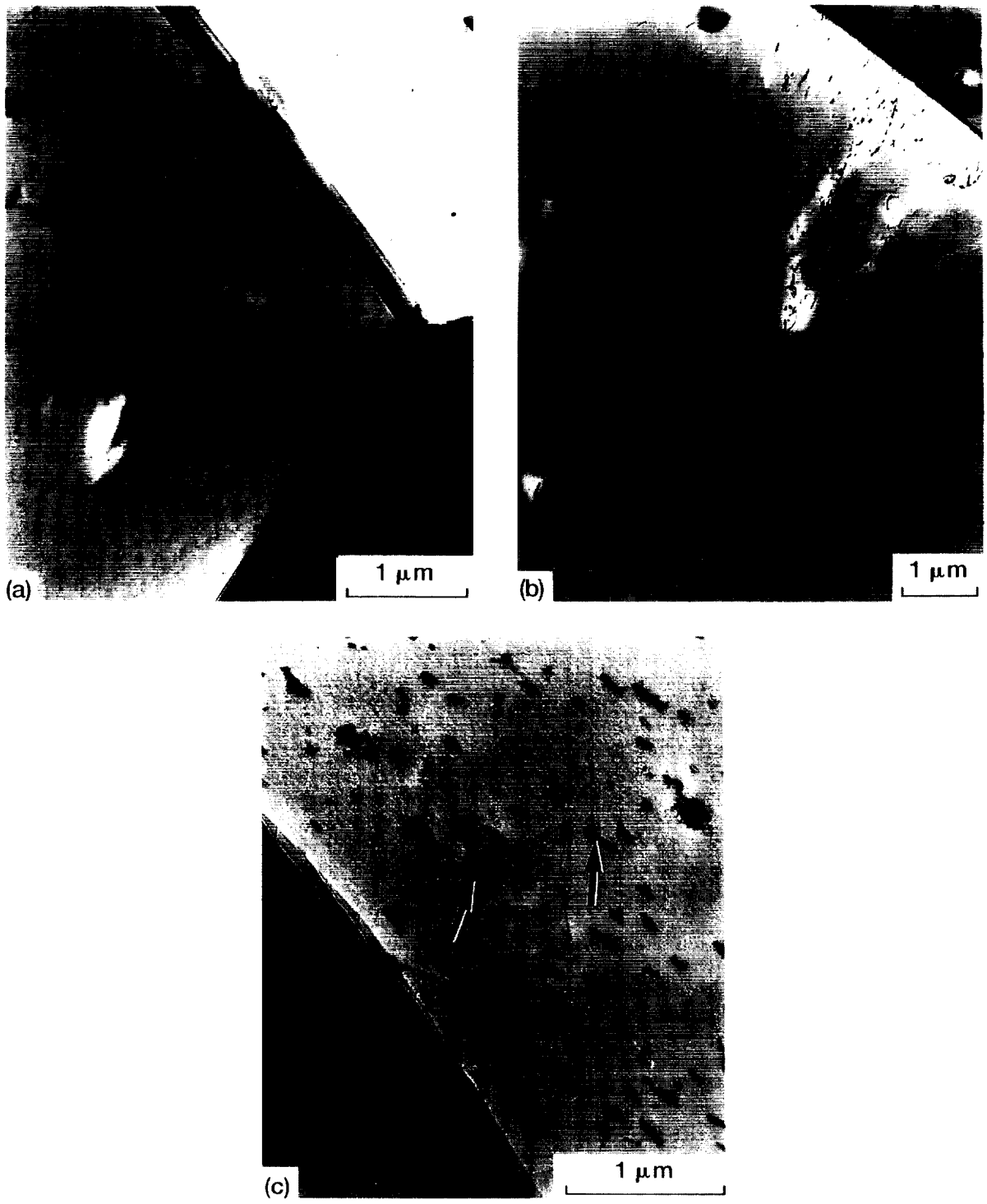

Fig. 12—TEM of Ni-50.6 Al specimens crept (*a*) and (*b*) to a true strain of 3.1 pct at 1200 K under a compressive engineering stress of 5.4 MPa, and (*c*) to a true strain 2.3 pct at 1300 K under a compressive engineering stress of 5.5 MPa. (a) An absence of dislocation substructure within most grains; (b) isolated bands of dislocation loops in a few grains; and (c) extrinsic grain-boundary dislocations and elongated loops in the matrix, where some are in the process of pinching off into smaller loops (arrows).

(class II) behavior, for which the dislocation climb velocity is slower than the viscous glide dislocation velocity.[26,28,29,31] However, it should be noted that the heterogeneous microstructure observed in this region (Figures (9) and (15)) and the absence of well-formed subgrains in all the grains, even after deformation to true strains of about 17 to 20 pct, indicate that dislocation climb occurs at much slower rates in NiAl than it does in pure metals, presumably due to the effects of long range order.

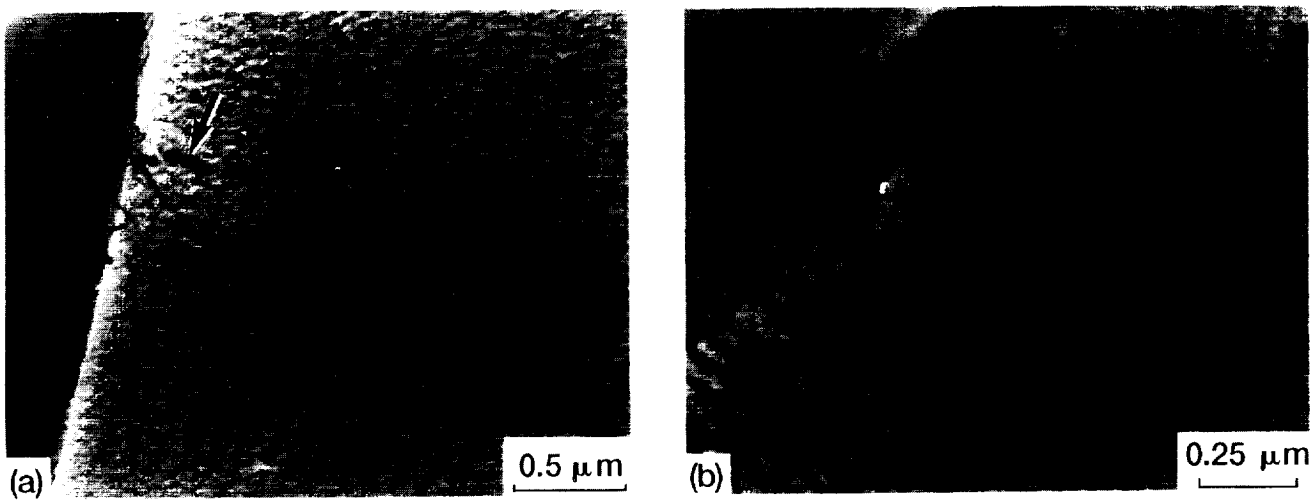

Fig. 13—TEM of a Ni-50.6 Al specimen crept to a true strain of 2.3 pct at 1300 K under a compressive engineering stress of 5.5 MPa showing (*a*) the emission of dislocation loops from an extrinsic grain-boundary dislocation dipole and the elongation and pinching off of a loop in the matrix (arrow); and (*b*) a high-magnification view of the same area shown in (a) under different tilt conditions. Note that the formation of the dislocation dipole has occurred by the reaction of two extrinsic grain-boundary dislocations.

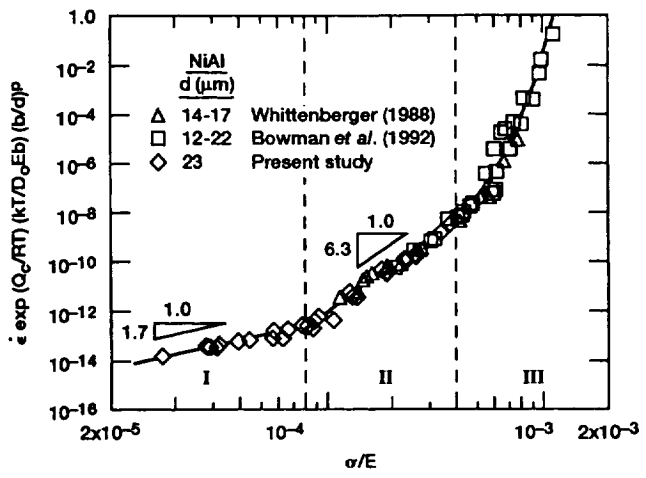

Fig. 14—Normalized creep rate *vs* normalized stress showing three creep regimes in powder-extruded Ni-50.6 Al. Data obtained from Whittenberger[13] for Ni-49.2 Al and Bowman *et al.*[25] for Ni-50.6 Al are compared with those obtained in the present investigation.

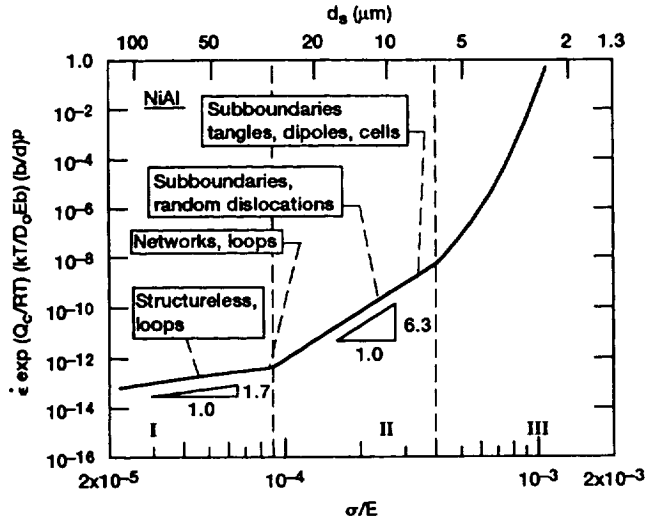

Fig. 15—Variation of the creep substructure in the power-law and low-stress creep regimes in powder-extruded Ni-50.6 Al shown schematically as a function of normalized creep rate and normalized stress.

A. *Comparison of the Low-Stress Mechanism with Theoretical Models*

Table III compares the general characteristics of Coble[36,37] and interface-controlled[38] creep mechanisms, as well as those for accommodated GBS proposed for superplastic materials[39] with those for the low-stress creep region. It is noted that several specific models exist for each of these mechanisms, but the values of A, n, p, and Q_c are similar to those given in Table III. An examination of the table indicates that the values of $A = 50$, $n = 1$, and $p = 3$ for Coble creep are vastly different from those observed in region I. Similarly, interface-controlled mechanisms predict $p = 1$ and $A = 730$, which are different from the constants for the new mechanism, although the predicted value of $n = 2$ agrees with the experimental results; the predicted magnitude of $Q_c = Q_s$, where Q_s is the activation energy for solute grain-boundary diffusion, would also be in agreement with experimental data if $Q_s \approx 100$ kJ mol^{-1} for NiAl. Clearly, the low-stress mechanism in region I is neither Coble creep nor an interface-controlled creep mechanism. Instead, the agreement between the experimental magnitudes of n, p, and Q_c and those predicted by models involving accommodated GBS[39] suggests that the latter is dominant in region I. However, the values of A predicted by these models, which typically lie between 75 and 150,[39] are over seven orders of magnitude larger than those determined experimentally (Table III). As a result, the predicted creep rates for models involving accommodated GBS are also over seven orders of

Table III. Comparison of Experimental and Theoretical Parameters for Region I

Mechanism	A	n	p	Q_c	References
Coble creep	50*	1	3	Q_{gb}	36 and 37
Interface-controlled creep	730	2	1	Q_s**	38
Accommodated GBS models	75 to 150	2	2	Q_{gb}	39
Experimental results	1.9×10^{-6}	2	2	Q_{gb}	present study

*Calculated assuming $\delta \approx 1.5\mathbf{b}$, where δ is the grain boundary width.
**Q_s is the activation energy for solute grain-boundary diffusion.

magnitude faster than the experimental creep rates, as shown in Figure 16, where the comparison is made with the Ball and Hutchinson model[40] to represent a typical superplastic model with $A \approx 100$;[39] the theoretical creep rates for most other superplastic models will lie within a factor of two of the line shown in Figure 16. The predicted trend for Coble creep, which is also shown in Figure 16, is similarly much higher than the experimental results by at least five orders of magnitude. Therefore, while accommodated GBS appears to be the dominant mechanism at low stresses in NiAl based on the magnitudes of n, p, and Q_c (Table III), none of the proposed models involving this process are in agreement with the experimental results. This inconsistency appears to be due to the fact that the theoretical models were developed for disordered materials and do not consider the effect of ordering on the accommodation mechanism and hence on the A parameter in Eq. [2].

The TEM observations reported in Section III–E–2 suggest significant grain-boundary dislocation activity during creep in the low-stress region (Figures 12(c) and 13(a) and (b)) which, in turn, should result in GBS. The presence of bands of dislocation loops in the matrix of some grains is intriguing (Figure 12(b)). It is believed that these loops are emitted into the matrix from the grain boundaries in order to accommodate GBS. Figures 13(a) and (b) suggest that extrinsic grain-boundary dislocations react to form dipoles during GBS, and these dipoles subsequently emit loops into the grain interior to accommodate stress concentrations developed in the boundary that result from sliding. A sequence consisting of loop elongation followed by its pinching-off into smaller loops (Figures 12(c) and 13(a) and (b)) appears to help in the generation and propagation of loops several microns away from the grain boundary (Figure 12(b)).

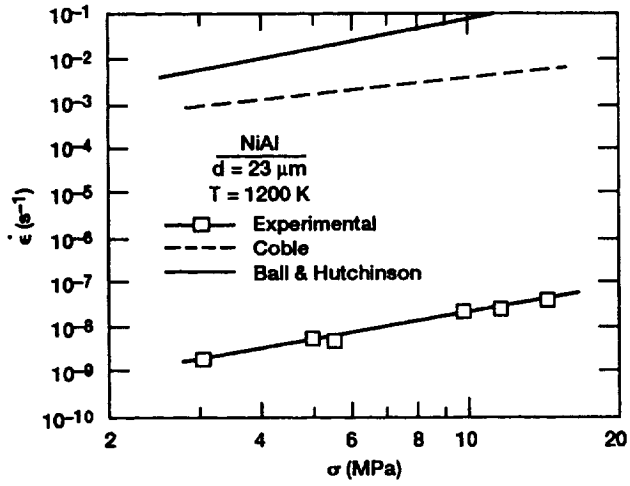

Fig. 16—Comparison between the experimental and predicted creep rates in the low-stress regime. The creep rates for Coble creep[36] and for the Ball and Hutchinson model[40] were calculated from the equations given in Refs. 37 and 39, respectively.

B. *Possible Implications of the Activation Energy Data on Grain-Boundary Structure*

Assuming that $Q_l \approx Q_{Ni}$, where Q_l is the activation energy for lattice self-diffusion in NiAl, and $Q_c \approx Q_{gb} \approx 100$ kJ mol^{-1}, it is interesting to note that the ratio $Q_{gb}/Q_l \approx 0.3$ is quite low as compared to ratios generally reported for pure metals for which $Q_{gb}/Q_l \approx 0.5$ to 0.7.[41] If this low value of Q_{gb}/Q_l is not due to scatter or impurity diffusion, the present results suggest that grain-boundary diffusion in NiAl is extremely rapid in comparison to pure metals, possibly due to easy diffusion paths at the boundaries. Based on their atomic calculations and computer simulations of $\Sigma 5$ [001](310) grain boundaries, Vitek and Chen[42] suggested that the grain boundaries of strongly ordered intermetallic alloys, such as Ni_3Al and NiAl, consist of columnar cavities that enable the preservation of chemical ordering in these materials up to the boundaries. Recent high resolution electron microscopy (HREM) observations and image analysis of the structure of $\Sigma 5$ [001](310) grain boundaries in NiAl reveal that they consist of 50 pct constitutional vacancies on the Ni sites and a mixture of 50 pct each of Ni antisite defects and constitutional vacancies on the Al sites adjacent to the boundary plane.[43] These two sets of results, while applicable to relatively simple symmetrical tilt boundaries, may provide a rationale for the low observed value of Q_{gb}/Q_l for NiAl if they are extended to other types of grain boundaries. In this case, the presence of interconnected columnar cavities or "nanotubes" along the grain-boundary plane is likely to allow vacancies to be channeled easily along the grain boundaries to dislocation sites. However, the grain boundaries in NiAl appear to be rich in Ni,[42] and this may suppress the formation of nanotubes in this alloy as compared to Ni_3Al.[44] Additional studies relating to grain-boundary structure and diffusion in NiAl are required to verify these hypotheses.

At first glance, it may appear that a low value of Q_{gb} for NiAl, which should lead to high creep rates, is inconsistent with the extremely low experimental values observed in region I (Figure 16). However, a careful consideration of the problem suggests that while a low ratio of Q_{gb}/Q_l indicates that GBS probably occurs much

more rapidly in NiAl than in pure metals, the low experimental creep rates observed in this material are primarily influenced by the magnitude of A, which is very low (Table III). This reasoning suggests that while long-range order in NiAl influences Q_{gb} through requiring the possible existence of nanotubes at the grain boundaries, its effect on the magnitude of A is much more significant.

V. SUMMARY AND CONCLUSIONS

The results obtained in the present study suggest that the creep data for NiAl fall into three regions.

1. Region I, a new creep regime that is grain-size dependent and exhibits $n \approx 2$, $Q_c \approx 100$ kJ mol^{-1}, and $p \approx 2$, is observed below $\sigma/E \approx 8 \times 10^{-5}$. A long primary creep region lasting over 100 hours for $\varepsilon \leq 1.5$ pct occurs in this regime, thereby indicating that it is a dislocation-controlled process. Transmission electron microscopy revealed considerable grain-boundary dislocation activity with most grain interiors being devoid of any dislocation substructure. However, a few grains showed bands of dislocation loops both at 1200 and 1300 K. These loops appear to have been emitted from the grain boundaries in order to accommodate GBS. Although most of the characteristics (*i.e.*, n, p, and Q_c) of region I agree with the values predicted by models for accommodated GBS developed for disordered materials, the experimental creep rates are over seven orders of magnitude lower than those predicted by theory. The ratio $Q_c/Q_l \approx Q_{gb}/Q_l \approx 0.3$ is much lower for NiAl than for pure metals. It is hypothesized that the grain boundaries of NiAl consist of vacancy flow channels or nanotubes resulting from long-range order. However, the influence of long-range order on the magnitude of A is significant enough to considerably lower the creep rates.
2. Power-law creep with $n \approx 6.5$ and $Q_c \approx 290$ kJ mol^{-1} is observed in region II between $\sigma/E \approx 8 \times 10^{-5}$ and 4×10^{-4}, where the shape of the primary creep region appears to be influenced by changes in dislocation mobility with temperature in this regime. The substructure in this creep regime consisted of a heterogeneous mixture of subboundaries, cells, random dislocations, dislocation loops, dipoles, and tangles. It is concluded that dislocation climb is the dominant mechanism in this region, although it is probably much slower than that in pure metals.
3. The activation energy for creep is stress dependent in region III, and $V^* \approx 100\ \mathbf{b}^3$ when $\sigma/E > 4 \times 10^{-4}$. An analysis of the data suggests that the power-law relation is no longer valid in this region. The dominating creep mechanisms in this region may involve processes other than dislocation climb, such as the cross slip of screw dislocations and obstacle-controlled glide. This is an area in which additional research is required.

REFERENCES

1. R.R. Vandervoort, A.K. Mukherjee, and J.E. Dorn: *Trans. ASM*, 1966, vol. 59, pp. 930-44.
2. W.R. Kanne, Jr., P.R. Strutt, and R.A. Dodd: *Trans. TMS-AIME*, 1969, vol. 245, pp. 1259-67.
3. P.R. Strutt and R.A. Dodd: in *Ordered Alloys: Structural Applications and Physical Metallurgy*, B.H. Kear, C.T. Sims, N.S. Stoloff, and J.H. Westbrook, eds., Claitor's Publishing Division, Baton Rouge, LA, 1970, pp. 475-504.
4. P.R. Strutt, R.A. Dodd, and G.M. Rowe: *2nd Int. Conf. on the Strength of Metals and Alloys*, ASM, Metals Park, OH, 1970, vol. III, pp. 1057-61.
5. L.A. Hocking, P.R. Strutt, and R.A. Dodd: *J. Inst. Met.*, 1971, vol. 99, pp. 98-101.
6. W.J. Yang and R.A. Dodd: *Met. Sci. J.*, 1973, vol. 7, pp. 41-47.
7. J. Bevk, R.A. Dodd, and P.R. Strutt: *Metall. Trans.*, 1973, vol. 4, pp. 159-66.
8. A. Prakash and M.J. Pool: *J. Mater. Sci.*, 1981, vol. 16, pp. 2495-2500.
9. M. Rudy and G. Sauthoff: *High-Temperature Ordered Intermetallic Alloys*, C.C. Koch, C.T. Liu, and N.S. Stoloff, eds., Materials Research Society, Pittsburgh, PA, 1985, vol. 39, pp. 327-33.
10. M. Rudy and G. Sauthoff: *Mater. Sci. Eng.*, 1986, vol. 81, pp. 525-30.
11. J.D. Whittenberger: *J. Mater. Sci.*, 1987, vol. 22, pp. 394-402.
12. I. Jung, M. Rudy, and G. Sauthoff: *High-Temperature Ordered Intermetallic Alloys II*, N.S. Stoloff, C.C. Koch, C.T. Liu, and O. Izumui, eds., Materials Research Society, Pittsburgh, PA, 1987, vol. 81, pp. 263-74.
13. J.D. Whittenberger: *J. Mater. Sci.*, 1988, vol. 23, pp. 235-40.
14. D.L. Yaney and W.D. Nix: *J. Mater. Sci.*, 1988, vol. 23, pp. 3088-98.
15. J.D. Whittenberger, R.K. Viswanadham, S.K. Mannan, and B. Sprissler: *J. Mater. Sci.*, 1990, vol. 25, pp. 35-44.
16. J.D. Whittenberger, K.S. Kumar, and S.K. Mannan: *J. Mater. Sci.*, 1991, vol. 26, pp. 2015-22.
17. K.R. Forbes, U. Glatzel, R. Darolia, and W.D. Nix: *High-Temperature Ordered Intermetallic Alloys V*, I. Baker, R. Darolia, J.D. Whittenberger, and M.H. Yoo, eds., Materials Research Society, Pittsburgh, PA, 1993, vol. 288, pp. 45-57.
18. U. Glatzel, K.R. Forbes, and W.D. Nix: *High-Temperature Ordered Intermetallic Alloys V*, Materials Research Society Symposia Proceedings, I. Baker, R. Darolia, J.D. Whittenberger, and M.H. Yoo, eds., Materials Research Society, Pittsburgh, PA, 1993, vol. 288, pp. 385-90.
19. K.R. Forbes and W.D. Nix: *High-Temperature Ordered Intermetallic Alloys V*, I. Baker, R. Darolia, J.D. Whittenberger, and M.H. Yoo, eds., Materials, Research Society, Pittsburgh, PA, 1993, vol. 288, pp. 749-55.
20. M.V. Nathal: in *Ordered Intermetallics—Physical and Mechanical Behaviour*, C.T. Liu, R.W. Cahn, and G. Sauthoff, eds., Kluwer Academic Publishers, Dordrecht, The Netherlands, 1992, pp. 541-63.
21. R.D. Noebe, R.R. Bowman, and M.V. Nathal: *Int. Mater. Rev.*, 1993, vol. 38, pp. 193-232.
22. D.B. Miracle: *Acta Metall. Mater.*, 1993, vol. 41, pp. 649-84.
23. G.F. Hancock and B.R. McDonnell: *Phys. Status Solidi*, 1971, vol. 4(a), pp. 143-50.
24. S.V. Raj and S.C. Farmer: *High-Temperature Ordered Intermetallic Alloys V*, I. Baker, R. Darolia, J.D. Whittenberger, and M.H. Yoo, eds., Materials Research Society, Pittsburgh, PA, 1993, vol. 288, pp. 647-52.
25. R.R. Bowman, R.D. Noebe, S.V. Raj, and I.E. Locci: *Metall. Trans. A*, 1992, vol. 23A, pp. 1493-1508.
26. W.D. Nix and B. Ilschner: in *Strength of Metals and Alloys*, P. Haasen, V. Gerold, and G. Kostorz, eds., Pergamon Press, Oxford, 1980, vol. 3, pp. 1503-30.
27. W.A. Coghlan, R.A. Menezes, and W.D. Nix: *Phil. Mag.*, 1971, vol. 23, pp. 1515-30.
28. H.J. Frost and M.F. Ashby: *Deformation-Mechanism Maps: The Plasticity and Creep of Metals and Ceramics*, Pergamon Press, Oxford, 1982.
29. J.E. Bird, A.K. Mukherjee, and J.E. Dorn: in *Quantitative Relations between Properties and Microstructure*, D.G. Brandon and A. Rosen, eds., University Press, Jerusalem, 1969, pp. 255-342.
30. M.R. Harmouche and A. Wolfenden: *J. Testing. Eval.*, 1987, vol. 15, pp. 101-04.
31. O.D. Sherby and P.M. Burke: *Prog. Mater. Sci.*, 1967, vol. 13, pp. 325-90.

32. H. Conrad: *J. Met.*, 1964, vol. 16, pp. 582-88.
33. A.G. Evans and R.D. Rawlings: *Phys. Status Solidi*, 1969, vol. 34, pp. 9-31.
34. S.V. Raj and G.M. Pharr: *Mater. Sci. Eng.*, 1986, vol. 81, pp. 217-37.
35. U. Glatzel, K.R. Forbes, and W.D. Nix: *Phil. Mag. A*, 1993, vol. 67, pp. 307-23.
36. R.L. Coble: *J. Appl. Phys.*, 1963, vol. 33, pp. 1671-73.
37. W.R. Cannon and T.G. Langdon: *J. Mater. Sci.*, 1988, vol. 23, pp. 1-20.
38. E. Artz, M.F. Ashby, and R.A. Verrall: *Acta Metall. Mater.*, 1983, vol. 31, pp. 1977-89.
39. R.C. Gifkins and T.G. Langdon: *Mater. Sci. Eng.*, 1978, vol. 36, pp. 27-33.
40. A. Ball and M.M. Hutchinson: *Met. Sci. J.*, 1969, vol. 3, pp. 1-7.
41. P.G. Shewmon: *Diffusion in Solids*, McGraw-Hill, New York, NY, 1963.
42. V. Vitek and S.P. Chen: *Scripta Metall. Mater.*, 1991, vol. 25, pp. 1237-42.
43. R.W. Fonda and D.E. Luzzi: *High-Temperature Ordered Intermetallic Alloys V*, I. Baker, R. Darolia, J.D. Whittenberger, and M.H. Yoo, eds., Materials Research Society, Pittsburgh, PA, 1993, vol. 288, pp. 361-66.
44. V. Vitek: University of Pennsylvania, Philadelphia, PA, private communication, 1993.